Applied Physics A (2020) 126:648
https://doi.org/10.1007/s00339-020-03842-6

Applied Physics A
Materials Science & Processing

Creep behavior and structure evolution of an advanced 9Cr-1.5Mo-1Co-VNbBN heat-resistant steel at elevated temperature

Jingen Gao[1] · **Zhizhong Dong**[2]

Received: 9 April 2020 / Accepted: 23 July 2020 / Published online: 31 July 2020

Abstract
The creep behavior and structure evolution of an advanced ultra-supercritical 9Cr-1.5Mo-1Co-VNbBN martensitic steel were investigated at temperatures of 620 °C and 650 °C. The microstructure before and after creep was observed by optical microscopy and transmission electron microscopy. It was shown that high temperature and high stress promoted the recovery of the laths and the growth of the secondary phases. The spheroidal precipitation of $M_{23}C_6$ within the sample which crept at 620 °C for 1994 h/5075 h and 650 °C for 942 h, grows continuously with increasing creep time and temperature, as results of atom diffusion at high temperature and plastic flow, while MX particles maintained high stability. Laves phase of Fe_2Mo precipitated and grew rapidly into large size of samples after the creep and aging exposure at 620 °C for 1994 h and more, resulting in a negative effect on the creep resistance of the steel.

Keywords Creep behavior · Microstructure evolution · Martensitic steel · Creep-resistant steel

1 Introduction

Martensitic creep-resistant steels have been widely used as various fossil power plant materials due to their high strength, good creep resistance and good antioxidative capacity at elevated-temperature. Over the past decades, the strength of these steels at high temperature has been improved significantly via the optimization of alloy composition [1, 2]. The present ultra-supercritical power plants utilize martensitic 9–12 wt% chromium steels for thick section components due to their larger thermal conductivity and lower thermal expansion as compared with austenitic steels [3]. The excellent mechanical properties at high temperature of these martensitic steels derive from solid solution strengthen from solution elements, high dislocation density induced by martensite phase transformation, stabilization of martensitic lath structure by kinds of precipitates, such as MX (M = V or Nb, and X = C or N), $M_{23}C_6$ and M_7C_3 (M = Cr or Fe), et al. [4, 5]. Among the various martensitic steels used at present, a series of 9Cr martensitic cast steels developed in the project of international collaboration with COST (Co-operation in the field of Science and Technology) program is one of the most promising classes [6]. The 9Cr martensitic cast steel (called CB2 in the COST program) containing 9%Cr, 1.0%Co, 1.5%Mo, 0.02%N and 0.01%B is one of them with the optimized composition through the addition of small quantities of boron. After normalizing and tempering, the microstructure of the steel commonly consists of tempered lath martensite without δ-ferrite or residual austenite and contains several types of particles including MX carbonitride within laths, and $M_{23}C_6$ carbides along lath boundaries as well as along prior austenite grain boundaries [7]. Production experiences of forgings, castings, and welding of this steel for an ultra-supercritical steam turbine have been reported, and investigations of aging and creep tests under low stress (a range from 50 to 120 MPa) have been carried out [8–10]. However, the properties and performance of this steel under higher stress and higher temperature are seldom studied. In this study, the creep behavior, especially the microstructure evolution at high stress and temperature of this advanced 9Cr steel were investigated and characterized. The role of stress and temperature on the microstructure and precipitates was also discussed.

✉ Jingen Gao
gaoje@tjnu.edu.cn

[1] College of Physics and Materials Science, Tianjin Normal University, Tianjin 300387, China

[2] School of Materials Science and Engineering, Tianjin University of Technology, Tianjin 300384, China

2 Experimental procedure

An alloy ingot with weight of 40 kg in the composition listed in Table 1 was produced by induction melting. The sectional drawing of the ingot is shown in Fig. 1a. The as-cast ingot was homogenized at 1070 °C for 10 h and cut into specimens with dimensions of 10 cm × 2 cm × 2 cm. Subsequently, the specimens were normalized at 1100 °C for 2 h followed by cooling in air and then tempered at 730 °C for 2 h, as shown schematically in Fig. 1b. The creep test specimens had a gauge length of 25 mm and a diameter of 5 mm. Creep rupture tests were performed at 620 and 650 °C with stresses of 170 and/or 120 MPa, respectively.

The microstructures and phase identification of the 9Cr steel were examined by optical microscopy (OM, Leica DM4000M), and the details of the structure of the samples were characterized by a transmission electron microscopy (TEM, JEOL JEM-2100F) with an energy dispersive X-ray spectrum (EDS). The TEM foils were mechanically ground to 30–50 μm thick followed by twinjet electro-polishing with a mixed solution of $HClO_4$:CH_3CH_2OH = 1:19.

3 Results

3.1 Tempered microstructure

The 9Cr steel tempered at 730 °C for 2 h had a tempered martensitic microstructure, as displayed in Fig. 2. The size of the prior austenite grains is approximately 100–150 μm (Fig. 2a). Figure 2b presents typical martensite laths with a width of 0.37 ± 0.04 μm. The tempering resulted in the formation of numerous rod-like and block-like particles identified as $M_{23}C_6$-type (M = Cr or Fe) precipitates, which mainly distributed at the lath boundaries and prior austenite grain boundaries (Fig. 2b). The average size of these $M_{23}C_6$ particles is about 95 ± 20 nm. In addition to $M_{23}C_6$ precipitates, massive plate-like MX-type (M = Nb or V, and X = C or N) carbonitrides with the size of about 10 nm can be observed within the martensitic lath matrix, as shown in Fig. 2c. The main metallic elements forming MX phase are Nb and V confirmed by EDS analysis (Fig. 2d). The dispersed fine particles could obstruct the movement of dislocations and the migration of the lath boundaries, leading to an improvement in microstructure stability and a reduction of the creep rate.

3.2 Creep behavior

Creep rupture tests of the 9Cr cast steel were conducted at 620 and 650 °C with applied stresses of 170 MPa and/or

Table 1 Composition of the 9Cr martensitic steel investigated (mass percent, %)

C	Cr	Co	Mn	Ni	Mo	V	Nb	Si	N	B	S	P	Fe
0.12	9.28	0.98	0.81	0.17	1.53	0.20	0.05	0.21	0.030	0.0088	0.002	< 0.005	Bal

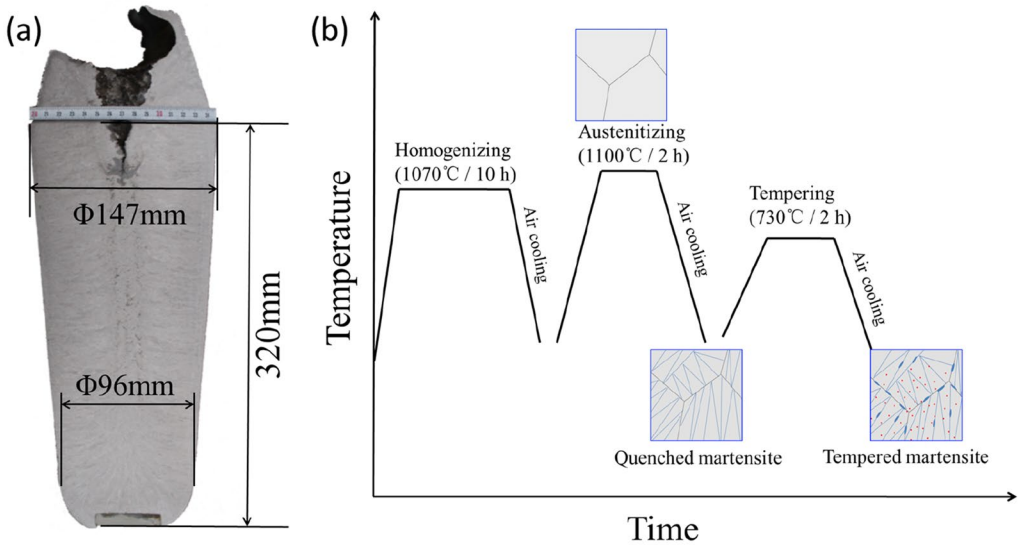

Fig. 1 **a** Sectional drawing of the ingot, and **b** heat treatment scheme

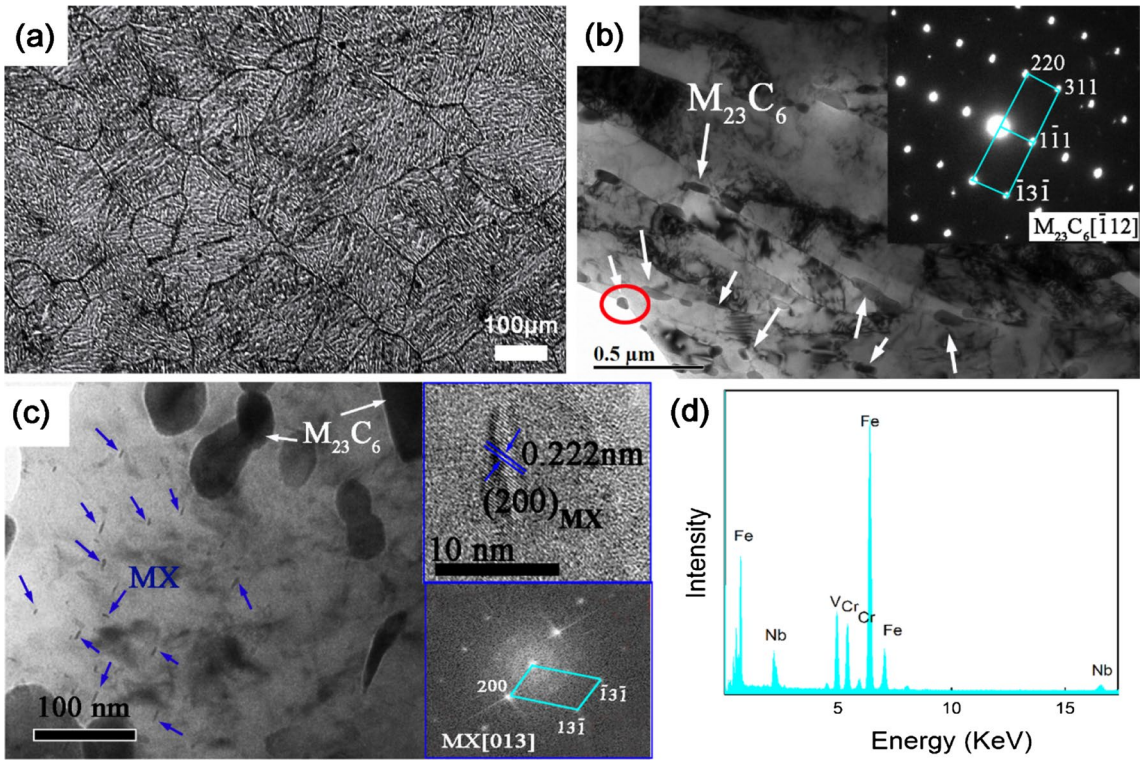

Fig. 2 OM and TEM images showing the microstructure of the 9Cr steel tempered at 730 °C for 2 h. **a** OM image, **b** TEM image showing the morphology of martensitic laths and $M_{23}C_6$ particles, the inset showing the electron diffraction pattern identified as $M_{23}C_6$ type phase, **c** TEM image showing the MX precipitates and the corresponding high-resolution TEM and local fast Fourier transform (FFT) analysis, and **d** EDX analysis from a particle of MX

120 MPa in air. The creep curves are displayed in Fig. 3a. Compared with previous studies [8, 9], the current testing conditions require higher temperature and greater stress. The times to rupture are 5075 h and 1994 h for the sample with stress of 120 MPa and 170 MPa at 620 °C, and it is 942 h for the sample with stress of 120 MPa at 650 °C, respectively. Figure 3b shows the creep rate, corresponding to strain per hour, vs. creep time for the steel. Typically, there are three stages of creep before fracture, consisting of the primary stage with a decreasing creep rate, secondary

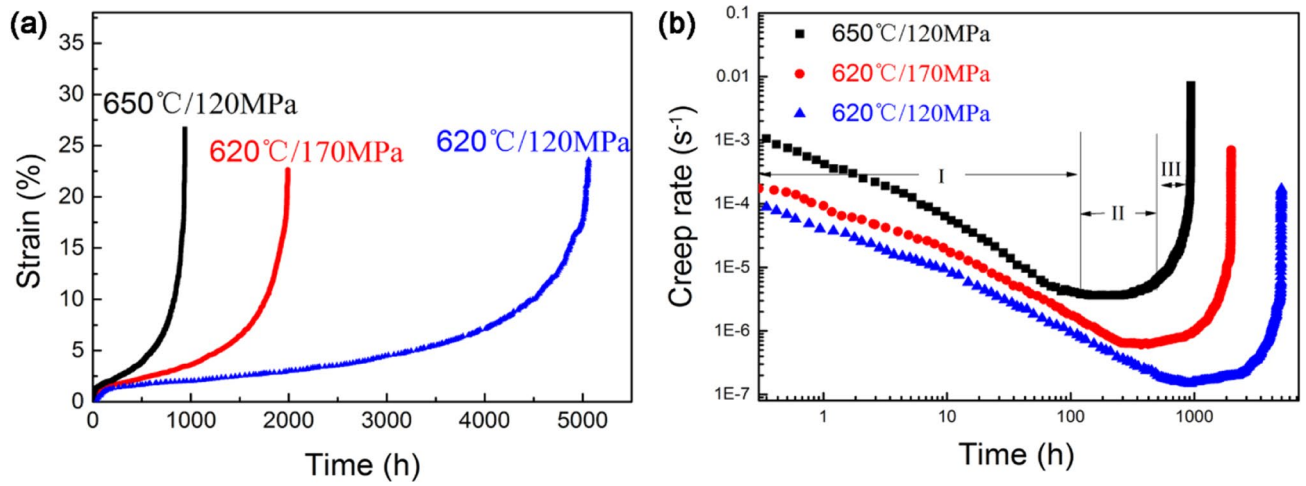

Fig. 3 **a** Creep curves and **b** the corresponding curves of creep rate vs. time for the 9Cr steel at 650 °C/120 MPa, 620 °C/170 MPa and 620 °C/120 MPa

stage with a steady and minimum creep rate and tertiary stage with an acceleration creep rate [11]. The three regimes can be observed in the curves of creep rate-time for this 9Cr steel, as shown in Fig. 3b. Figure 4 shows a Larson–Miller parameter (LMP) of this steel, in comparison with that of several heat-resistant martensitic steels, including P91B with 120 ppm boron, 10Cr-2 W-3Co-MoNbVNB with 30 ppm nitrogen, GX12CrMoWVNbN10-1-1 with 500 ppm nitrogen [12–14]. Figure 4 reveals that long term rupture strength of the studied 9Cr steel may be marginally better or at least comparable to that of those traditional heat-resistant steels.

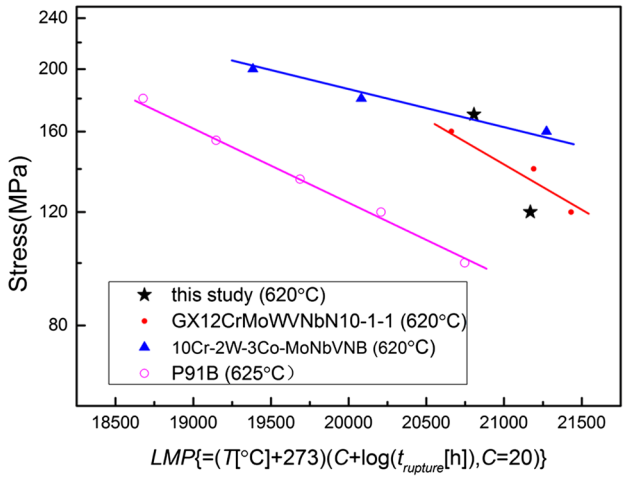

Fig. 4 Larson–Miller parameter (LMP) of the studied steel plotted as a function of stress, in comparison with that of several heat-resistant martensitic steels (data from [12–14])

3.3 Microstructure evolution

Figures 5 and 6 show the microstructure observed by TEM of the gauge section near the fracture and grip portion of the samples after creep rupture at 620 °C/170 MPa and 620 °C/120 MPa, respectively. The initial structure of tempered martensite is replaced by equiaxed grains/subgrains in the gauge section of samples after creep, as present in Figs. 5a and 6a. During creep process, due to the continuous movement and annihilation of dislocations in the matrix and at the lath boundaries, the laths are recovered, and subgrains are formed. The mean sizes of the $M_{23}C_6$ increase to 143 ± 35 nm and 102 ± 30 nm in the samples crept at 620 °C/170 MPa and 620 °C/120 MPa, which is obviously larger than that in tempered condition, respectively. However, MX particles which precipitated during the tempering treatment seem stable against coarsening without obvious variety after creep (Figs. 5c, 6c, 7b, c). Moreover, as a result of long-term

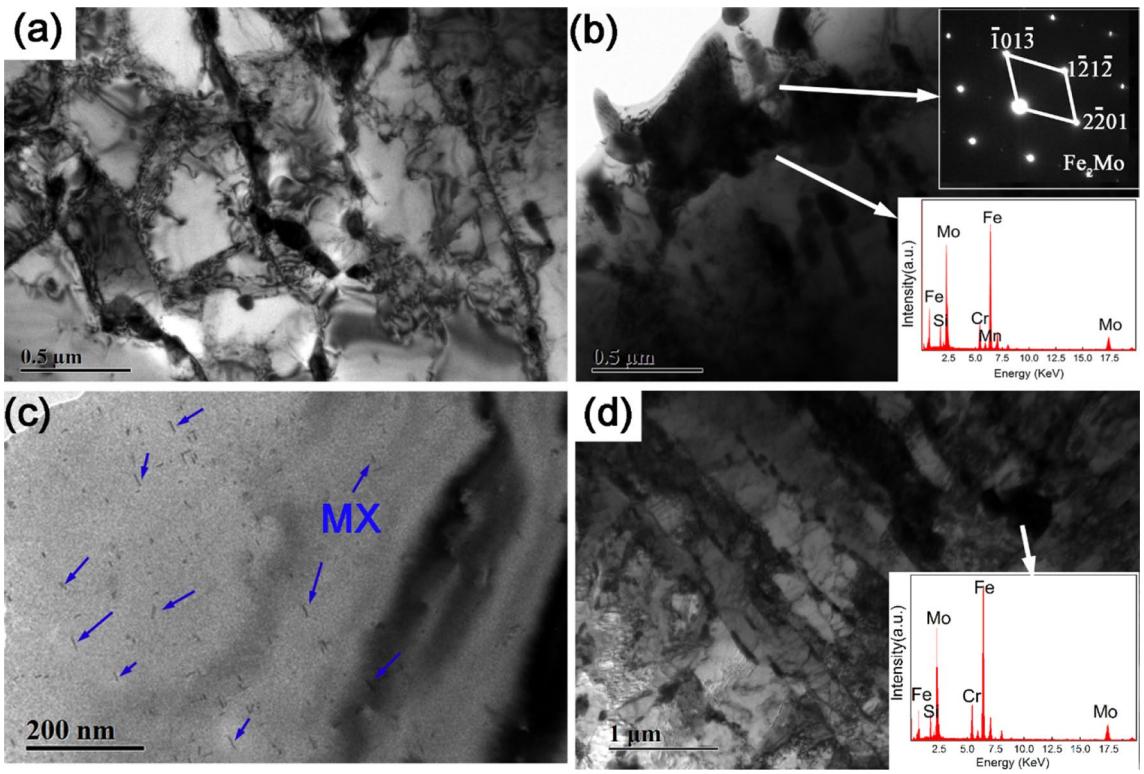

Fig. 5 TEM images of microstructures after creep at 620 °C under 170 MPa, **a** subgrains, **b** particles of Fe_2Mo Laves phase, the insets are the corresponding electron diffraction pattern and EDX spectrum, **c** particles of MX, **d** the microstructure of the location of the specimen head (stress-free aging) and the EDX spectrum of the Laves phase

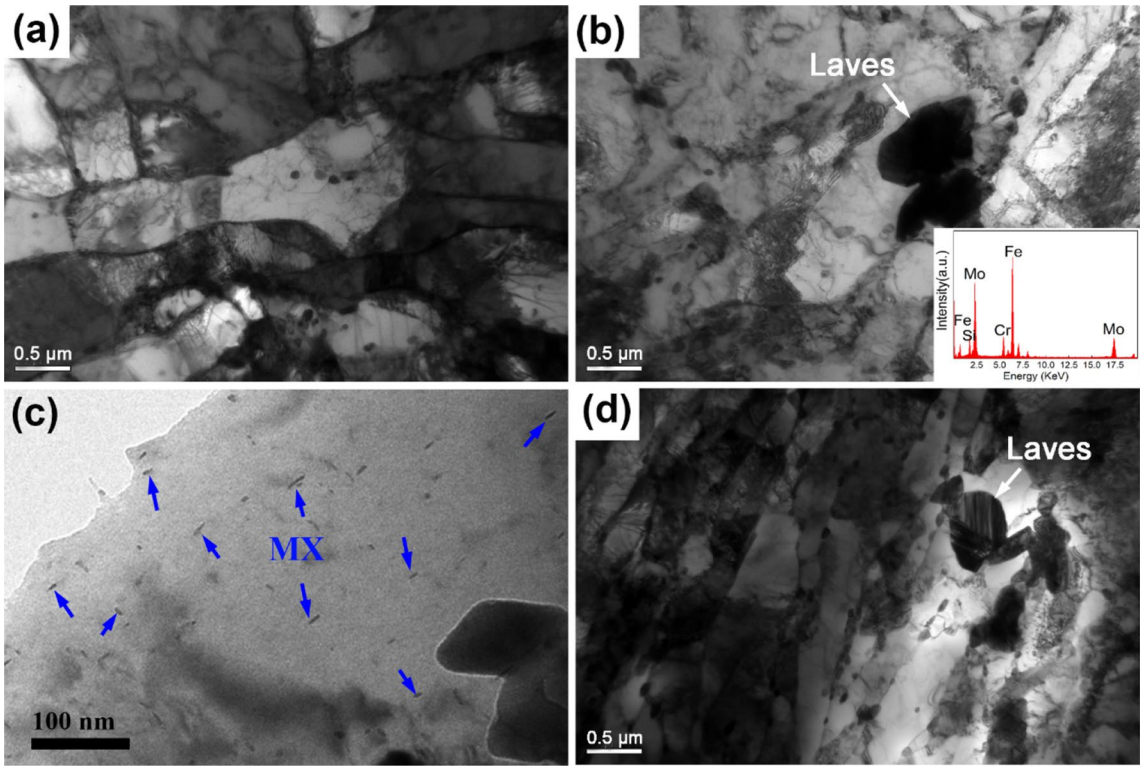

Fig. 6 TEM images of microstructures after creep at 620 °C under 120 MPa, **a** subgrains, **b** Laves phase of Fe_2Mo and the corresponding EDX spectrum, **c** particles of MX, **d** the microstructure of the location of the specimen head (stress-free aging)

creep and aging, Laves phase of Fe_2Mo was indicated in both the gauge section (Figs. 5b, 6b) and grip portion (Figs. 5d, 6d) of the specimen [7]. It can be seen that the size of the Laves phase exceeds 0.5 μm, which is much larger than that of $M_{23}C_6$ particles. Generally, the Laves phase precipitated long after the $M_{23}C_6$ particles in 9Cr steels, implying that the growing rate of Laves phase was faster than that of $M_{23}C_6$ particles [15]. In sample crept at 650 °C, as shown in Fig. 7, the coarsening of $M_{23}C_6$ precipitates were also evident (163 ± 42 nm), whereas the Laves phase was not detected in neither the crept sample nor the stress-free aging sample. The microstructural parameters including sizes of MX, $M_{23}C_6$ and Laves phase particles, and the transverse size of martensite laths were summarized in Table 2.

4 Discussion

Generally, the stress and strain at high-temperature results in recovery of laths and increasing size of subgrains [16]. The samples crept at 620 °C and 650 °C were characterized by a remarkable change of structure, as shown in Figs. 5a, 6a and 7a. Grip portions of samples after creep rupture at 620 °C and 650 °C were also examined to make clear the changes of microstructure during aging without effect by stress and plastic deformation, as shown in Figs. 5d, 6d and 7d, respectively. In grip portions without stress, the martensitic lath structure is retained, and the lath width does not change significantly. The lath boundary is thermally stable, and no transformation of lath into subgrain can be found in the grip portion. The $M_{23}C_6$ particles seem to be stable, and the size of them does not increase significantly during the aging without stress and deformation. Compared to the microstructure in the stress section, the microstructure evolution of the stress-free portion is distinctly slower. The growth of subgrains during the creep process occurs concurrently with the coarsening of the secondary phase of $M_{23}C_6$ precipitates, as a result of plastic flow at elevated temperature. Stress and strain in the gauge section, which in comparison with the stress-free grip portion, could accelerate the coarsening rate of $M_{23}C_6$ particles. Sawada et al. found that free dislocation in lath interior and boundaries could move under loading and deformation, and these dislocations could act as diffusion pipes with fast mobile for atoms when they move to the particles [17]. The coarsening rate of particles is accelerated by the fast diffusion of atoms. Moreover, plastic flow induced by stress not only increases the number of moving dislocations but also promotes their movement. Consequently, $M_{23}C_6$ particles have large sizes in the gauge section, and the subgrains replace the martensitic laths though

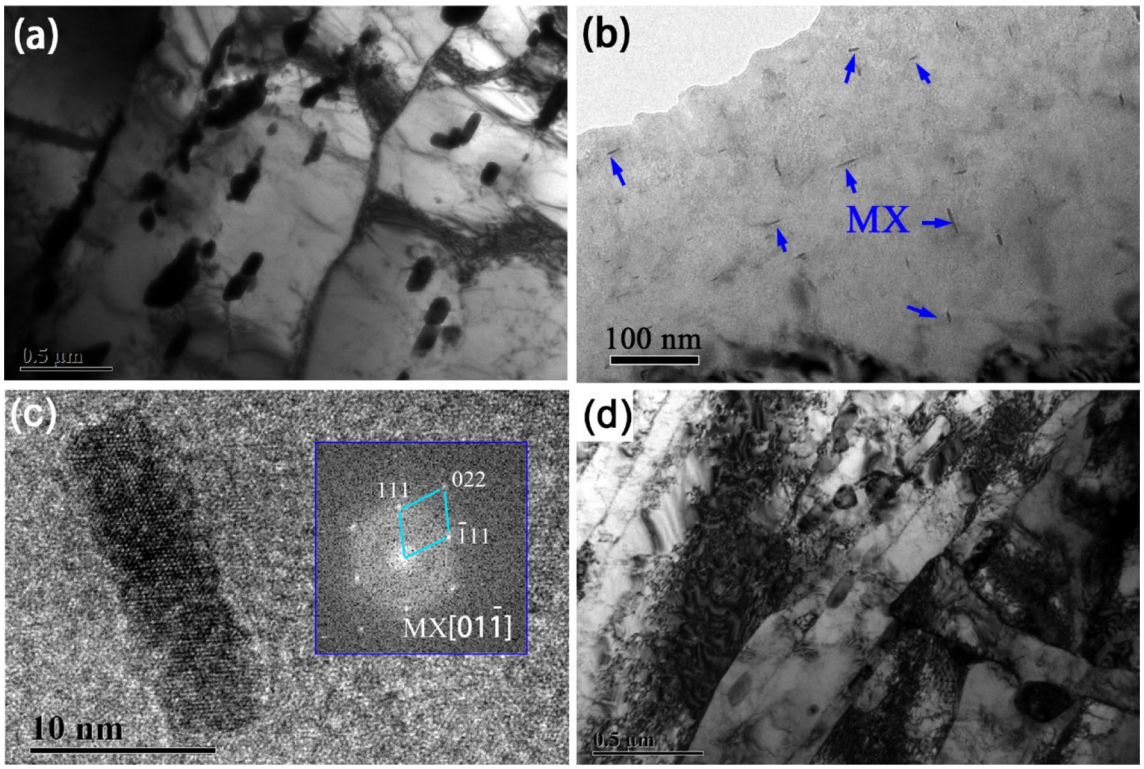

Fig. 7 TEM images of microstructures after creep at 650 °C under 120 MPa, **a** subgrains, **b** particles of MX, **c** an high-resolution TEM graph and the corresponding FFT analysis of a MX particle, **d** the microstructure of the location of the specimen head (stress-free aging)

Table 2 Variation of the microstructural parameters

Samples	Tempered	620 °C/1994 h	620 °C/5075 h	650 °C/942 h
$M_{23}C_6$ (nm)	95 ± 20	143 ± 35	102 ± 30	163 ± 42
MX (nm)	10 ± 3	12 ± 3	13 ± 4	13 ± 4
Laves (nm)	–	580 ± 70	650 ± 100	–
Martensite lath (μm)	0.37 ± 0.04	0.45 ± 0.06	0.55 ± 0.10	0.60 ± 0.10

dislocation migration [18]. Generally, MX particles are very stable against coarsening during creep at temperature below 650 °C [19, 20]. In this study, no apparent change in the fraction and size of MX particles was detected after creep at 620 °C and 650 °C. The influence of stress in the gauge section is pronounced only for $M_{23}C_6$ particles [15].

It is worth noting that Laves phase significant coarsens under conditions of creep and aging and the size is almost the same under the two conditions, demonstrating that the nucleation and growth of the Laves phase depend on the exposure duration of creep/aging at high temperature [21]. With the increase in exposure duration of high temperature, the Laves phase begins to precipitate and coarsen rapidly. Generally, the Laves phase nucleates along the martensitic lath boundary or around the $M_{23}C_6$ carbide, and its growth process consumes the alloy elements in the matrix or $M_{23}C_6$ carbide in close vicinity due to the rearrangement of the alloy elements (Cr, Mo, et al.), which reduce the strengthening effect of solid solution elements and carbides in the matrix [22, 23]. Due to the large volume (micron scale) and wide space of Laves particles, they provide slight contributions to the creep strength of the steel in the creep process of high temperature, and the interface between the matrix and Laves phase often becomes the crack source, resulting in material failure [21].

5 Conclusions

Creep behavior and microstructure evolution of the 9Cr martensitic cast steel strengthened by $M_{23}C_6$ and nano-sized MX were scrutinized. The following conclusions can be drawn. Microstructure evolution occurring during the creep process was characterized by the recovery of the laths and the

formation of subgrains. High temperature and high stress promoted the growth of $M_{23}C_6$ particles, while the nano-sized MX particles maintain an extremely high stability. Laves phase has been found not only in the creep section but also in the long-term aging portion, after exposure at 620 °C for 1994 h and more. The sizes of most of the Laves phase exceed 0.5 μm, resulting in a negative effect on the creep resistance of the steel.

Acknowledgements This work was financially supported by the National Natural Science Foundation of China (Grant No. 51901157 and 51771137), Tianjin Science and Technology Project (17YFZCGX00900) and the Ph.D. startup foundation of Tianjin Normal University (043135202-XB1710).

References

1. F. Masuyama, ISIJ Int. **41**, 612 (2001)
2. F. Abe, M. Taneike, K. Sawada, Int. J. Press. Vessels Pip. **84**, 3 (2017)
3. F. Abe, Engineering **1**, 211 (2015)
4. V. Dudko, A. Belyakov, D. Molodov, R. Kaibyshev, Metall. Mater. Trans. A. **44**, 162 (2013)
5. M. Mikami, Mater. Sci. Technol. **33**, 1074 (2017)
6. T. Kern, M. Staubli, B. Scarlin, ISIJ Int. **42**, 1515 (2002)
7. J. Gao, Z. Dong, H. Ren, B. Ning, X. Xu, Z. Chen, Steel Res. Int. **90**, 1800534 (2019)
8. R. Vanstone, I. Chilton, P. Jaworski, J. Eng. Gas Turbines Power **135**, 062101 (2013)
9. D. Jandova, J. Kasl, E. Chvostova, Mater. Sci. Forum. **782**, 311 (2014)
10. S. Baumgartner, H. Pahr, T. Zauchner, Weld World **62**, 811 (2018)
11. F. Abe, in Creep-resistant steels, ed. by F. Abe, T. Kern, R. Viswanathan (Woodhead Publishing Limited, Cambridge, 2008) pp. 3–6
12. N. Dudova, R. Mishnev, R. Kaibyshev, Mater. Sci. Eng. A **766**, 138353 (2019)
13. Y.I. Borisova, V.A. Dudko, V.N. Skorobogatykh, I.A. Shchenkova, R.O. Kaibyshev, Phys. Met. Metall. **118**, 1022 (2017)
14. J. Baral, J. Swaminathan, R.N. Ghosh, Procedia Eng **55**, 88 (2013)
15. P. Hofer, H. Cerjak, B. Schaffernak, P. Warbichler, Steel Res. **69**, 343 (1998)
16. E. Tkachev, A. Belyakov, R. Kaibyshev, Mater. Sci. Eng. A **725**, 228 (2018)
17. K. Sawada, K. Kubo, F. Abe, Mater. Sci. Eng. A **319–321**, 784 (2001)
18. P. Hu, W. Yan, W. Sha, W. Wang, Y. Shan, K. Yang, J. Mater. Sci. Technol. **27**, 344 (2011)
19. A. Gustafson, M. Hattestrand, Mater. Sci. Eng. A **333**, 279 (2002)
20. C.G. Panait, A. Zielinska-Lipiec, T. Koziel, A. Czyrska-Filemonowicz, A. Gourgues-Lorenzon, W. Bendick, Mater. Sci. Eng. A **527**, 4062 (2010)
21. I. Fedorova, A. Belyakov, P. Kozlov, V. Skorobogatykh, I. Shenkova, R. Kaibyshev, Mater. Sci. Eng. A **615**, 153 (2014)
22. H. Cui, F. Sun, K. Chen, L. Zhang, R. Wan, A. Shan, J. Wu, Mater. Sci. Eng. A **527**, 7505 (2010)
23. Y. Xu, M. Wang, Y. Wang, T. Gu, L. Chen, X. Zhou, Q. Ma, Y. Liu, J. Huang, J Alloys Compd. **621**, 93 (2015)